arXiv:1406.3924v2 [cond-mat.mes-hall] 15 Dec 2014

Unusual electronic properties of clean and disordered zigzag graphene nanoribbons

J M Luck[1] **and Y Avishai**[2]

[1] Institut de Physique Théorique, URA 2306 of CNRS, CEA Saclay, 91191 Gif-sur-Yvette cedex, France

[2] Department of Physics and the Ilse Katz Center for Nano-Science, Ben-Gurion University, Beer-Sheva 84105, Israel

E-mail: jean-marc.luck@cea.fr,yshai@bgu.ac.il

Abstract. We revisit the problem of electron transport in clean and disordered zigzag graphene nanoribbons, and expose numerous hitherto unknown peculiar properties of these systems at zero energy, where both sublattices decouple because of chiral symmetry. For clean ribbons, we give a quantitative description of the unusual power-law dispersion of the central energy bands and of its main consequences, including the strong divergence of the density of states near zero energy, and the vanishing of the transverse localization length of the corresponding edge states. In the presence of off-diagonal disorder, which respects the lattice chiral symmetry, all zero-energy localization properties are found to be anomalous. Recasting the problem in terms of coupled Brownian motions enables us to derive numerous asymptotic results by analytical means. In particular the typical conductance g_N of a disordered sample of width N and length L is shown to decay as $\exp(-C_N w\sqrt{L})$, for arbitrary values of the disorder strength w, while the relative variance of $\ln g_N$ approaches a non-trivial constant K_N. The dependence of the constants C_N and K_N on the ribbon width N is predicted. From the mere viewpoint of the transfer-matrix formalism, zigzag ribbons provide a case study with many unusual features. The transfer matrix describing propagation through one unit cell of a clean ribbon is not diagonalizable at zero energy. In the disordered case, we encounter non-trivial random matrix products such that all Lyapunov exponents vanish identically.

1. Introduction

Ever since the experimental discovery of graphene, the list of its amazing properties increases without let-off [1, 2, 3, 4]. These range from technological aspects, graphene being a light and strong material that conducts charge and heat and can be integrated into many devices, to fundamental features, such as Dirac cones near zero energy, relativistic physics at $v_F \ll c$, Klein paradox, zero-energy Landau level, and many others.

Investigating electronic properties in the bulk, i.e., for an infinite 2D sheet of graphene, is relatively simple because translation invariance holds in both directions. But an infinite system is an idealization, and, sooner or later, one faces the task of analyzing electronic properties of finite (or semi-infinite) systems, and especially systems with boundaries. This is important if one is interested, for example, in the integration of graphene into an electrical circuit or any other device. The difference of electronic properties between a bulk infinite graphene sheet and a system with boundaries such as a nanoribbon is dramatic. In particular the presence of boundaries may completely modify the spectrum and the structure of its Dirac points. The energy dispersion is indeed known to be intimately related with the geometry of the boundaries [2, 3, 4].

It therefore comes as no surprise that, since the early days of graphene, an extensive research has been devoted to electronic properties of systems with boundaries in general, and to nanoribbons in particular [5, 6, 7, 8, 9, 10, 11, 12, 13, 14, 15, 16, 17, 18, 19, 20]. Nanoribbons are obtained by cutting a stripe out of the 2D graphene sheet along two parallel lines, such that translation invariance is maintained along the stripe. The main possible edge structures are zigzag, armchair and bearded. Electronic properties of graphene ribbons with zigzag edges have been shown to exhibit several peculiar features at zero energy. At this special energy, right at the band center, both sublattices decouple because of chiral symmetry, and the system exhibits flat bands and exponentially localized edge states [2, 6, 7, 9, 11, 14, 15, 17, 20]. Zero energy is also usually the Fermi energy, if the system is neither doped or gated.

In the present work we revisit this problem in a self-contained way, considering successively clean and disordered zigzag ribbons within the one-particle tight-binding framework. This study will unveil many novel features of these systems at zero energy. The unusual power-law dispersion of the central bands provides the leading thread which unites all these properties.

The setup of this paper is as follows. Section 2 is devoted to clean zigzag ribbons. In Section 2.1 we give a fully self-contained account of their band structure and edge states. We emphasize the power-law dispersion of the two central bands around zero energy, and several of its consequences. For a ribbon of width N, i.e., consisting of N coupled chains, this dispersion law reads $E \approx \pm Q^N$, where $Q = \pi - q$ is the momentum difference relative to the boundary of the Brillouin zone. Surprisingly, this unusual dispersion law, with its exponent equal to the ribbon width N, was previously noticed only in a single recent unpublished work [17]. Section 2.2 contains an investigation of generic zero-energy eigenstates of a semi-infinite ribbon. The structure of a special zero-energy state that has a unit amplitude on the upper left corner of the ribbon reveals a peculiar pattern where the amplitudes build up a Pascal triangle. In Section 3 we turn to the investigation of zero-energy properties of zigzag ribbons in the presence of hopping (off-diagonal) disorder. Our main motivation for choosing this type of disorder is theoretical: off-diagonal disorder respects the so-called chiral symmetry

between both sublattices. It may therefore be expected to keep some of the very peculiar zero-energy features of clean ribbons. Moreover, hopping disorder might be induced by applying a weak inhomogeneous strain, as hopping integrals have a strong exponential dependence on interatomic distances (see [21]). We shall investigate in particular the distribution of generic zero-energy eigenstates in Section 3.1 and of the zero-energy conductance in Section 3.2, using the transfer-matrix approach to the electronic conductance of quasi-one-dimensional systems, which has been developed in the early days of mesoscopic physics [22, 23, 24, 25, 26]. Recasting the problem in terms of coupled Brownian motions evolving in a fictitious continuous time $\tau = w^2 l$ enables us to derive by analytical means asymptotically exact predictions for many quantities of interest, for an arbitrary disorder strength w. As a general rule, all observables related to localization properties are anomalous. A typical zero-energy wavefunction on a semi-infinite ribbon exhibits an anomalous sub-exponential growth with the distance l from the end of the ribbon, scaling as $\exp(A_n w\sqrt{l})$ on chain number n. The typical conductance g_N of a finite disordered ribbon of width N and length L exhibits an anomalous sub-exponential decay with L, scaling as $\exp(-C_N w\sqrt{L})$. Band-center anomalies in quasi-one-dimensional bipartite systems with off-diagonal disorder in the tight-binding formalism have been studied long ago, first in the case of chains [27, 28, 29, 30, 31], and then for rectangular strips made of N coupled channels for odd N [32, 33, 34, 35]. In the present situation, the source of anomalous behavior is different. Unusual behaviour is predicted at zero energy, irrespective of the number of channels, either even or odd. Section 4 contains a brief discussion of our main findings. In Appendix A we employ elementary methods to study zero-energy properties of a single chain, while Appendix B is devoted to the statistics of zero-energy eigenstates at chain number $n = 2$.

2. Clean ribbons

A zigzag graphene nanoribbon consists of N coupled chains, as shown in Figure 1 for $N = 3$. It is a periodic array whose unit cell (blue box) contains $2N$ sites. Sites are conveniently labelled $i = (m, l)$, where $m = 1, \ldots, 2N$ is the site number within a cell, while l is the cell number along the ribbon. The ribbon is bipartite, with even and odd m corresponding to the two equivalent sublattices, each cell containing N even sites and N odd sites.

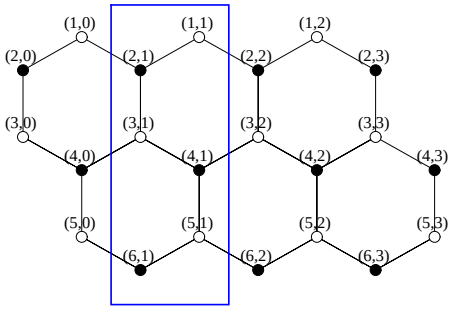

Figure 1. A zigzag nanoribbon of width $N = 3$. Blue box: unit cell containing 6 sites, 3 even ones (full symbols) and 3 odd ones (empty symbols).

2.1. Band structure

Zigzag ribbons have been known for long to have unusual electronic properties [2, 6, 7, 9, 11, 14, 15, 17, 20]. The existence of localized edge states at zero energy and the flatness of the central bands near the boundaries of the Brillouin zone are the most salient of these characteristic properties, which are absent in other geometries, such as armchair ribbons or nanotubes.

Let us begin with a self-contained direct derivation of the band structure of zigzag ribbons, without using the two-dimensional band structure of the graphene sheet. We consider the one-particle tight-binding Hamiltonian

$$\mathcal{H} = \sum_{<i,j>} (a_i^\dagger a_j + a_j^\dagger a_i), \tag{2.1}$$

where the sum runs over pairs of nearest neighbors, and the hopping amplitude has been set to unity. For an eigenstate at energy E, the amplitudes $\psi_{m,l}$ obey

$$\begin{aligned} E\psi_{4k+1,l} &= \psi_{4k,l} + \psi_{4k+2,l} + \psi_{4k+2,l+1}, \\ E\psi_{4k+2,l} &= \psi_{4k+1,l-1} + \psi_{4k+1,l} + \psi_{4k+3,l}, \\ E\psi_{4k+3,l} &= \psi_{4k+2,l} + \psi_{4k+4,l-1} + \psi_{4k+4,l}, \\ E\psi_{4k+4,l} &= \psi_{4k+3,l} + \psi_{4k+3,l+1} + \psi_{4k+5,l}. \end{aligned} \tag{2.2}$$

Let us consider an infinitely long ribbon and look for Bloch states of the form

$$\begin{aligned} \psi_{4k+1,l} &= \phi_{4k+1}\, \mathrm{e}^{\mathrm{i}ql}, \\ \psi_{4k+2,l} &= \phi_{4k+2}\, \mathrm{e}^{\mathrm{i}q(l-1/2)}, \\ \psi_{4k+3,l} &= \phi_{4k+3}\, \mathrm{e}^{\mathrm{i}q(l-1/2)}, \\ \psi_{4k+4,l} &= \phi_{4k+4}\, \mathrm{e}^{\mathrm{i}ql}, \end{aligned} \tag{2.3}$$

where the longitudinal momentum q is in the first Brillouin zone ($|q| \leq \pi$). The transverse amplitudes ϕ_m obey the relations

$$\begin{aligned} E\phi_{2n+1} &= \phi_{2n} + \gamma\phi_{2n+2}, \\ E\phi_{2n+2} &= \gamma\phi_{2n+1} + \phi_{2n+3}, \end{aligned} \tag{2.4}$$

with

$$\gamma = 2\cos\frac{q}{2}. \tag{2.5}$$

We thus obtain an effective q-dependent tight-binding model on a finite dimerized chain of $2N$ sites [2, 17], as shown in Figure 2. The hopping amplitudes originating from vertical bonds (single black lines) equal unity, whereas those originating from pairs of oblique bonds (double red lines) equal γ.

Figure 2. Effective dimerized chain corresponding to the ribbon shown in Figure 1. Single black lines: unit hopping amplitudes. Double red lines: γ hopping amplitudes.

Looking for a solution to (2.4) of the form

$$\begin{aligned} \phi_{2n+1} &= A\, \mathrm{e}^{\mathrm{i}np}, \\ \phi_{2n+2} &= B\, \mathrm{e}^{\mathrm{i}np}, \end{aligned} \tag{2.6}$$

where p is the transverse momentum, we obtain the transverse dispersion relation

$$E^2 = 1 + 2\gamma \cos p + \gamma^2 \tag{2.7}$$

and the quantization condition

$$\sin Np + \gamma \sin(N+1)p = 0. \tag{2.8}$$

The above equations [2, 15, 17] possess two kinds of solutions.

- *Bulk states*, corresponding to real values of p, are transversely extended. Their energies read

$$E = \pm \frac{\sin p}{\sin(N+1)p}. \tag{2.9}$$

- *Edge states*, corresponding to complex values of p, of the form $p = \pi + \mathrm{i}\kappa$, are exponentially localized in the transverse direction ($\phi_{2n+1} \sim \phi_{2n+2} \sim (-1)^n \mathrm{e}^{\pm n\kappa}$). The existence of localized edge states has been known for long [2, 6, 7, 11, 14, 15, 17]. In the present framework, we have

$$\sinh N\kappa = \gamma \sinh(N+1)\kappa \tag{2.10}$$

  and the corresponding energies read

$$E = \pm \frac{\sinh \kappa}{\sinh(N+1)\kappa}. \tag{2.11}$$

The resulting band structure is shown in Figure 3 for $N = 6$. Edge states only contribute to the wings of the central bands. More precisely, for $|q| < q_N$, with

$$\cos \frac{q_N}{2} = \frac{N}{2(N+1)}, \tag{2.12}$$

all the bands correspond to bulk states. In the wings of the Brillouin zone ($|q| > q_N$), the two central bands correspond to edge states. Both expressions (2.9) and (2.11) agree to give $E = \pm 1/(N+1)$ at the transition points $q = \pm q_N$ (symbols).

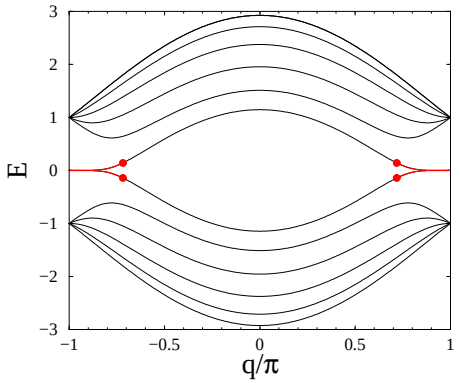

Figure 3. Band structure of the zigzag ribbon for $N = 6$. Black: bulk states. Red: edge states. Red symbols: transition points ($q = \pm q_N$).

The transverse localization length ξ of the edge states is obtained by taking the $N \to \infty$ limit in (2.10). We thus obtain [6, 7, 11, 14, 15, 17]

$$\frac{1}{\xi} = \kappa = \ln \frac{1}{\gamma} = \ln \frac{1}{2\cos(q/2)}. \tag{2.13}$$

The localization length ξ diverges at the threshold for the occurrence of edge states, $q_\infty = \lim q_N = 2\pi/3$. This simple result can be predicted by means of a topological argument based on the Zak phase [16].

It is worth scrutinizing the vicinity of the boundaries of the Brillouin zone. Right at the boundaries ($q = \pm\pi$), the hopping amplitude γ vanishes, and so the dimerized chain splits up into $(N-1)$ dimers and two isolated atoms at the endpoints. Now, setting $|q| = \pi - Q$, with Q small, we have

$$\gamma \approx Q, \quad \kappa \approx \ln \frac{1}{Q}. \tag{2.14}$$

The pairs of dimer levels ($E = \pm 1$) hybridize to give $2(N-1)$ bands of bulk states, with $p \approx a\pi/N$, and so

$$E \approx \pm \left(1 + Q \cos \frac{a\pi}{N}\right) \quad (a = 1, \ldots, N-1). \tag{2.15}$$

The two atomic levels ($E = 0$) give rise to the central bands of edge states. Equations (2.11) and (2.14) yield

$$E \approx \pm Q^N. \tag{2.16}$$

The wings of the central bands therefore obey an unusual power-law dispersion, whose exponent is the ribbon width N, and whose prefactor is exactly unity. This result, which has far reaching consequences, seems to have been noticed so far only in [17].

The contribution of the central bands to the density of states per site therefore diverges as a power law as $E \to 0$, for any $N \geq 2$, according to

$$\rho(E) \approx \frac{1}{2\pi N} \frac{\mathrm{d}Q}{\mathrm{d}E} \approx \frac{|E|^{-(N-1)/N}}{2\pi N^2}. \tag{2.17}$$

This divergence explains the observed unusual behavior [7] of the flatness index η, defined as the portion of the central bands contained in a small energy interval $|E| < \Delta$ around zero energy. We indeed predict

$$\eta \approx N \int_{-\Delta}^{\Delta} \rho(E)\, \mathrm{d}E \approx \frac{\Delta^{1/N}}{\pi}. \tag{2.18}$$

Another consequence of the power-law dispersion (2.16) is the vanishing of the transverse localization length ξ of the edge states as $E \to 0$, according to

$$\frac{1}{\xi} \approx \ln \frac{1}{Q} \approx \frac{1}{N} \ln \frac{1}{|E|}. \tag{2.19}$$

2.2. Generic zero-energy eigenstates

The above analysis of the band structure demonstrates that zero energy is very peculiar, as it coincides with the endpoints of the two central bands of edge states, with the power-law dispersion (2.16). On an infinitely long ribbon, the Hamiltonian (2.1) has only two zero-energy Bloch states, one living on each sublattice:

$$\psi_{1,l} = (-1)^l \quad \text{and} \quad \psi_{2N,l} = (-1)^l. \tag{2.20}$$

These states are strictly confined at the edges, in agreement with the fact that $\xi \to 0$ as $E \to 0$ (see (2.19)).

It is therefore natural to wonder what generic zero-energy eigenstates look like, besides the above Bloch states which live on an infinitely long, translationally invariant ribbon. The goal of this section is to investigate this question in detail.

As expected from chiral symmetry, the tight-binding equations (2.2) on both sublattices decouple at zero energy. Furthermore, they can be recast into the recursive form

$$\begin{aligned} \psi_{4k+2,l+1} &= -\psi_{4k,l} - \psi_{4k+2,l}, \\ \psi_{4k+4,l+1} &= -\psi_{4k+2,l+1} - \psi_{4k+4,l}, \end{aligned} \tag{2.21}$$

$$\begin{aligned} \psi_{4k+3,l+1} &= -\psi_{4k+3,l} - \psi_{4k+5,l}, \\ \psi_{4k+1,l+1} &= -\psi_{4k+3,l+1} - \psi_{4k+1,l}. \end{aligned} \tag{2.22}$$

For definiteness, we consider a semi-infinite ribbon starting with cell number $l = 0$ and extending infinitely far to the right. Furthermore, we focus our attention onto the even sublattice. The recursion relations (2.21) can be solved as follows.

- For $n = 2$, we have $\psi_{2,l+1} = -\psi_{2,l}$, and so
$$\psi_{2,l} = (-1)^l \psi_{2,0}. \tag{2.23}$$
The initial condition $\psi_{2,0}$ is arbitrary.
- For $n = 4$, we have $\psi_{4,l+1} = -\psi_{2,l+1} - \psi_{4,l}$, and so
$$\psi_{4,l} = (-1)^{l+1}(l+1)\psi_{2,0}. \tag{2.24}$$
In particular $\psi_{4,0} = -\psi_{2,0}$.
- For $n = 6$, we have $\psi_{6,l+1} = -\psi_{4,l} - \psi_{6,l}$, and so
$$\psi_{6,l} = (-1)^l \Big(\psi_{6,0} - \frac{1}{2}\, l(l+1)\psi_{2,0} \Big). \tag{2.25}$$
The initial condition $\psi_{6,0}$ is arbitrary.
- For $n = 8$, we have $\psi_{8,l+1} = -\psi_{6,l+1} - \psi_{8,l}$, and so
$$\psi_{8,l} = (-1)^{l+1} \Big((l+1)\psi_{6,0} - \frac{1}{6}\, l(l+1)(l+2)\psi_{2,0} \Big). \tag{2.26}$$
In particular $\psi_{8,0} = -\psi_{6,0}$.

The above results show the structure of a generic zero-energy eigenstate on the even sublattice of a semi-infinite ribbon. The arbitrary initial values are those at the leftmost column of sites, i.e., $\psi_{4k+2,0}$. The amplitudes grow as various powers of the distance l along the ribbon. The fastest growth is proportional to the initial condition $\psi_{2,0}$.

It is worth considering in more detail the special eigenstate obtained if the only non-zero initial condition at $l = 0$ is $\psi_{2,0} = 1$. This special zero-energy eigenstate is remarkable. Its amplitudes build up a Pascal triangle. In other words, they can be expressed in terms of binomial coefficients:

$$\begin{aligned} \psi_{4k+2,l} &= (-1)^{k+l} \binom{k+l}{2k}, \\ \psi_{4k+4,l} &= (-1)^{k+l+1} \binom{k+l+1}{2k+1}. \end{aligned} \tag{2.27}$$

A similar construction of a symmetric zero-energy eigenstate induced by a single defect has been given in [19]. This special eigenstate is shown in Figure 4 for $N = 6$.

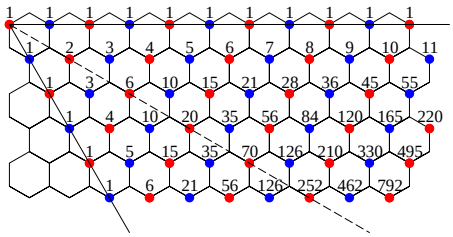

Figure 4. Special zero-energy eigenstate on the even sublattice of a semi-infinite ribbon for $N = 6$. Red symbols: positive amplitudes. Blue symbols: negative amplitudes. Full lines: boundaries of the eigenstate. Dashed line: symmetry axis.

Positive (resp. negative) amplitudes are shown as red (resp. blue) symbols. Full lines show the boundaries of the eigenstate, where amplitudes equal ± 1. The dashed line shows the symmetry axis of the eigenstate ($l = 3k$ or $3k + 1$). The amplitudes of the special eigenstate grow as successive powers of l:

$$|\psi_{2n,l}| \approx \frac{l^{n-1}}{(n-1)!}. \tag{2.28}$$

The fastest growth is observed for $n = N$, i.e., at the lower edge of the ribbon. The eigenstate thus becomes more and more strongly localized at the lower edge as one goes deeper and deeper into the semi-infinite ribbon. This observation goes hand in hand with the strict confinement of the zero-energy Bloch states (2.20) at the edges, and with the fact that $\xi \to 0$ as $E \to 0$ (see (2.19)).

A few words about the relation of the above eigenstates to the usual notion of a normalizable wavefunction are in order. Generic generic eigenstates solve the zero-energy one-boundary problem, where we impose the amplitudes at one end of a semi-infinite ribbon and propagate the solution by the tight-binding equations or, equivalently, by the transfer matrix. The eigenstates thus constructed are not normalizable in general. This should not be a surprise, as they do not solve the standard (two-boundaries) Sturm-Liouville problem. In the presence of off-diagonal disorder, generic eigenstates will be shown to grow subexponentially with distance l (see (3.24)).

3. Disordered ribbons

We now turn to the study of electronic properties of zigzag ribbons with off-diagonal disorder. The corresponding Hamiltonian reads

$$\mathcal{H} = \sum_{<i,j>} t_{ij}(a_i^\dagger a_j + a_j^\dagger a_i), \tag{3.1}$$

where the sum runs over pairs of nearest neighbors, and the hopping amplitudes t_{ij} are independent random variables. This type of disorder respects the lattice chiral symmetry. It may therefore be expected to keep some of the peculiar zero-energy features of clean ribbons. Tight-binding Hamiltonians with off-diagonal disorder on some other bipartite structures [30], including chains [27, 28, 29, 31] and strips [32, 33, 34, 35], have been shown to exhibit anomalous localization at zero

energy. Throughout this section, we focus our attention onto zero-energy properties. We parametrize the hopping amplitudes as

$$t_{ij} = \mathrm{e}^{\varepsilon_{ij}}, \tag{3.2}$$

where the ε_{ij} are independent random variables, drawn from an unspecified symmetric probability distribution with zero mean and variance w^2: $\overline{\varepsilon_{ij}} = 0$, $\mathrm{var}\,(\varepsilon_{ij}) = w^2$. The positive parameter w thus represents the disorder strength.‡

For convenience, we introduce the notations

$$u_{n,l} = \exp\bigl(\varepsilon^{(u)}_{n,l}\bigr), \quad v_{n,l} = \exp\bigl(\varepsilon^{(v)}_{n,l}\bigr), \quad w_{n,l} = \exp\bigl(\varepsilon^{(w)}_{n,l}\bigr) \tag{3.3}$$

for the hopping amplitudes attached to various types of bonds, as shown in Figure 5.

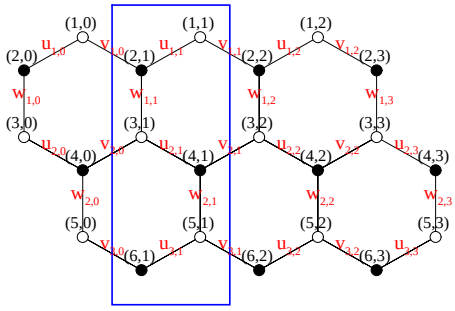

Figure 5. Notations for the hopping amplitudes attached to various bonds.

3.1. Zero-energy eigenstates

In this section we investigate the behavior of generic zero-energy eigenstates of the disordered Hamiltonian (3.1), following the line of thought of Section 2.2. At zero energy, the disordered tight-binding equations can be recast into a recursive form generalizing (2.21) and (2.22):

$$\begin{aligned} v_{2k+1,l}\psi_{4k+2,l+1} &= -w_{2k,l}\psi_{4k,l} - u_{2k+1,l}\psi_{4k+2,l}, \\ u_{2k+2,l+1}\psi_{4k+4,l+1} &= -w_{2k+1,l+1}\psi_{4k+2,l+1} - v_{2k+2,l}\psi_{4k+4,l}, \end{aligned} \tag{3.4}$$

$$\begin{aligned} v_{2k+2,l}\psi_{4k+3,l+1} &= -u_{2k+2,l}\psi_{4k+3,l} - w_{2k+2,l}\psi_{4k+5,l}, \\ u_{2k+1,l+1}\psi_{4k+1,l+1} &= -w_{2k+1,l+1}\psi_{4k+3,l+1} - v_{2k+1,l}\psi_{4k+1,l}. \end{aligned} \tag{3.5}$$

Here again, we consider a semi-infinite ribbon starting with unit number $l = 0$, and extending infinitely far to the right, and we focus our attention onto the even sublattice. It is advantageous to reformulate the recursion relations (3.4) as difference equations. To do so, let us introduce the products

$$U_{n,l} = \prod_{m=0}^{l-1} u_{n,m}, \quad V_{n,l} = \prod_{m=0}^{l-1} v_{n,m}. \tag{3.6}$$

‡ Hereafter the bar denotes an average over the disorder, and we use the notation $\mathrm{var}\,(X) = \overline{X^2} - \overline{X}^2$ for the disorder variance of a quantity X.

Setting

$$\begin{aligned}\psi_{4k+2,l} &= (-1)^{k+l}\frac{U_{2k+1,l}}{V_{2k+1,l}}S_{4k+2,l},\\ \psi_{4k+4,l} &= (-1)^{k+l+1}\frac{V_{2k+2,l}}{U_{2k+2,l+1}}S_{4k+4,l},\end{aligned} \tag{3.7}$$

we obtain

$$\begin{aligned}S_{4k+2,l+1} - S_{4k+2,l} &= \frac{V_{2k,l}V_{2k+1,l}}{U_{2k,l+1}U_{2k+1,l+1}}\,w_{2k,l}S_{4k,l},\\ S_{4k+4,l+1} - S_{4k+4,l} &= \frac{U_{2k+1,l+1}U_{2k+2,l+1}}{V_{2k+1,l+1}V_{2k+2,l+1}}\,w_{2k+1,l+1}S_{4k+2,l+1}.\end{aligned} \tag{3.8}$$

These difference equations can again be solved recursively.

- For $n = 2$, we have

$$\psi_{2,l} = (-1)^l\frac{U_{1,l}}{V_{1,l}}\psi_{2,0}, \tag{3.9}$$

  i.e., $S_{2,l} = \psi_{2,0}$, where the initial condition $\psi_{2,0}$ is arbitrary.

- For $n = 4$, we have

$$\psi_{4,l} = (-1)^{l+1}\frac{V_{2,l}}{U_{2,l+1}}S_{4,l}, \tag{3.10}$$

  with

$$S_{4,l} = \sum_{m=0}^{l-1}\frac{U_{1,m}U_{2,m}}{V_{1,m}V_{2,m}}\,w_{1,m}\psi_{2,0}. \tag{3.11}$$

  In particular $S_{4,0} = w_{1,0}\psi_{2,0}$ and $\psi_{4,0} = -(w_{1,0}/u_{2,0})\psi_{2,0}$.

It is again worth considering the special zero-energy eigenstate on the even sublattice for which the initial condition is $\psi_{m,0} = \delta_{m,2}$. In this situation, it is clear from their recursive definition that all the quantities $S_{2n,l}$ are positive. As a consequence, the amplitudes $\psi_{2n,l}$ of the special eigenstate on a disordered ribbon have exactly the same signs as expressions (2.27), irrespective of the realization of disorder, i.e., of the draw of the hopping rates t_{ij}.

The analysis of the growth law of the magnitudes $|\psi_{2n,l}|$ goes as follows. Beginning with $n = 2$, we consider the quantity

$$X_{1,l} = \ln|\psi_{2,l}| = \ln\frac{U_{1,l}}{V_{1,l}} = \sum_{m=0}^{l-1}\left(\varepsilon_{1,m}^{(u)} - \varepsilon_{1,m}^{(v)}\right). \tag{3.12}$$

The rightmost side is the sum of $2l$ independent random variables with zero mean and variance w^2. We have therefore

$$\overline{\ln|\psi_{2,l}|} = 0, \quad \mathrm{var}\,(\ln|\psi_{2,l}|) = 2w^2 l. \tag{3.13}$$

For a large distance l, by the central limit theorem, $X_{1,l}$ is asymptotically a Gaussian variable with zero mean and variance $2w^2 l$. More generally, for arbitrary k, all the quantities

$$X_{2k+1,l} = \ln\frac{U_{2k+1,l}}{V_{2k+1,l}}, \quad X_{2k+2,l} = \ln\frac{V_{2k+2,l}}{U_{2k+2,l}} \tag{3.14}$$

are asymptotically independent Gaussian variables with zero mean and variance $2w^2 l$.

It is advantageous to recast (3.7) and (3.8) in terms of the latter variables. We thus obtain

$$\begin{aligned} |\psi_{4k+2,l}| &= \mathrm{e}^{X_{2k+1,l}}\, S_{4k+2,l}, \\ |\psi_{4k+4,l}| &= \mathrm{e}^{X_{2k+2,l}}\, \frac{1}{u_{2k+2,l}} S_{4k+4,l}, \end{aligned} \tag{3.15}$$

and

$$\begin{aligned} S_{4k+2,l+1} - S_{4k+2,l} &= \mathrm{e}^{-X_{2k+1,l}}\, \frac{w_{2k,l}}{u_{2k+1,l}}\, |\psi_{4k,l}|\,, \\ S_{4k+4,l+1} - S_{4k+4,l} &= \mathrm{e}^{-X_{2k+2,l+1}}\, w_{2k+1,l+1}\, |\psi_{4k+2,l+1}|\,. \end{aligned} \tag{3.16}$$

For large distances ($l \gg 1$), the Gaussian variables $X_{n,l}$, which enter (3.15) and (3.16) exponentially, are typically large. They are also slowly varying with distance l, in the sense that the differences $X_{n,l+1} - X_{n,l}$ have finite variances $2w^2$. These observations justify the following simplifying steps.

(i) It is legitimate to use a continuum approximation, replacing the discrete distance l by the fictitious continuous time

$$\tau = w^2 l. \tag{3.17}$$

The quantities $X_{n,l}$ become independent Gaussian processes $X_n(\tau)$, known as *Brownian motions*, such that

$$\overline{X_n(\tau)} = 0, \quad \mathrm{var}\,(X_n(\tau)) = 2\tau. \tag{3.18}$$

The connection between off-diagonal disorder at zero energy and random walks (or Brownian motions, which are nothing but the continuum limit thereof) has been known for long in the case of a single chain [27, 28, 29, 31].

(ii) Within this continuum framework, consistently discarding all prefactors of order unity, (3.15) and (3.16) can be merged into the integral recursions

$$|\psi_{2n,l}(\tau)| \approx \mathrm{e}^{X_n(\tau)} \int_0^\tau \mathrm{e}^{-X_n(\tau')}\, |\psi_{2n-2,l}(\tau')|\, \mathrm{d}\tau'. \tag{3.19}$$

The latter equations can be solved recursively in terms of the $X_n(\tau)$, as

$$\begin{aligned} |\psi_{2,l}(\tau)| &\approx \mathrm{e}^{X_1(\tau)}, \\ |\psi_{4,l}(\tau)| &\approx \mathrm{e}^{X_2(\tau)} \int_0^\tau \mathrm{e}^{X_1(\tau')-X_2(\tau')} \mathrm{d}\tau', \\ |\psi_{6,l}(\tau)| &\approx \mathrm{e}^{X_3(\tau)} \int_0^\tau \mathrm{e}^{X_2(\tau')-X_3(\tau')} \mathrm{d}\tau' \\ &\qquad \times \int_0^{\tau'} \mathrm{e}^{X_1(\tau'')-X_2(\tau'')} \mathrm{d}\tau'', \end{aligned} \tag{3.20}$$

and so on.

(iii) The growth of the amplitudes $|\psi_{2n,l}|$ can be estimated by evaluating the nested integrals entering (3.20) by the saddle-point method, i.e., by looking for the times $\tau', \tau'', \ldots$ which maximize the integrands. We thus obtain

$$\ln |\psi_{2n,l}| \approx M_n(\tau) + X_n(\tau), \tag{3.21}$$

where the $M_n(\tau)$ are non-trivial random processes, defined by the recursion relation

$$M_n(\tau) = \max_{0 \le \tau' \le \tau} \left(M_{n-1}(\tau') + X_{n-1}(\tau') - X_n(\tau')\right), \tag{3.22}$$

with $M_1(\tau) = 0$. The processes $M_n(\tau)$ inherit the diffusive scaling of the Brownian motions $X_n(\tau)$ which generate them. We have therefore in particular

$$\overline{M_n(\tau)} = A_n\sqrt{\tau}, \quad \mathrm{var}\,(M_n(\tau) + X_n(\tau)) = B_n\tau, \tag{3.23}$$

where the amplitudes A_n and B_n are constants which depend only on the chain number n.

We are thus left with the asymptotic growth laws

$$\overline{\ln|\psi_{2n,l}|} \approx A_n w\sqrt{l}, \quad \mathrm{var}\,(\ln|\psi_{2n,l}|) \approx B_n w^2 l. \tag{3.24}$$

These formulas are the main result of this section. They hold for all values of the disorder strength w. We thus predict that a generic zero-energy eigenstate grows subexponentially with distance l on a disordered ribbon. This growth follows a power law on a clean ribbon (see (2.28)). We shall come back in the discussion to the connection between the growth laws (2.28) and (3.24) and the transfer-matrix formalism. We have not succeeded in evaluating exactly the constants A_n and B_n, except in the following two cases. For $n = 1$, the result (3.13) yields the simple results

$$A_1 = 0, \quad B_1 = 2. \tag{3.25}$$

For $n = 2$, the problem boils down to the distribution of the maximum of a single Brownian motion (see Appendix B). We thus obtain

$$A_2 = \sqrt{\frac{8}{\pi}}, \quad B_2 = 4 - \frac{8}{\pi}. \tag{3.26}$$

For higher n, we have obtained numerical values of A_n and B_n by means of a direct simulation of the coupled random processes $X_n(\tau)$ and $M_n(\tau)$. Figure 6 shows plots of A_n^2 and $1/B_n^3$ against chain number n, up to $n = 100$. The good quality of the linear fits strongly suggests that A_n and B_n scale for large n as

$$A_n \approx 2.8\sqrt{n}, \quad B_n \approx 1.6\, n^{-1/3}. \tag{3.27}$$

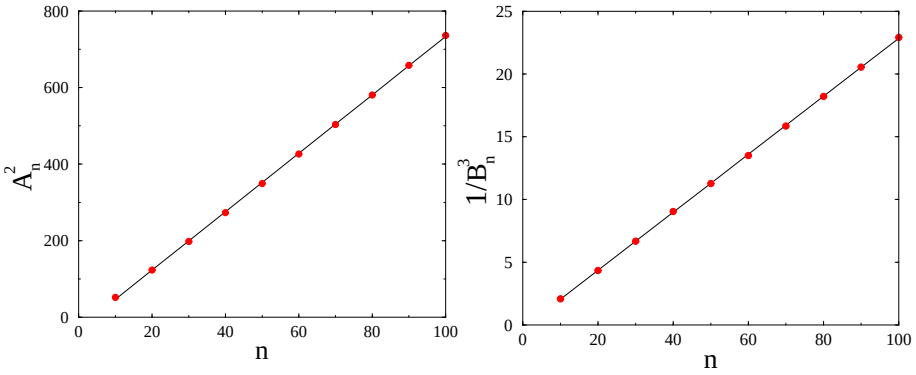

Figure 6. Plots of A_n^2 and $1/B_n^3$ against chain number n. Straight lines: least-square fits with respective slopes 7.63 and 0.231.

In order to illustrate the above results, Figure 7 shows the special zero-energy eigenstate on the even sublattice of semi-infinite disordered ribbons of width $N = 4$. The hopping rates are drawn from the uniform distribution in the interval $-\sqrt{3} \leq$

$\varepsilon \leq \sqrt{3}$, corresponding to a disorder strength $w = 1$. Colors code for five different realizations of disorder. The four panels show plots of $\ln|\psi_{2n,l}|$ against the distance l along each chain. Smooth lines show averages of the plotted quantities over many samples, growing asymptotically as $A_n\sqrt{l}$ (see (3.24)). For $n = 1$, the tracks behave as Brownian motions and have zero average. For higher n (other panels), averages increase with n (in agreement with the slow growth of A_n with n), while individual tracks show less and less dispersion around the averages (in agreement with the slow fall-off of B_n with n).

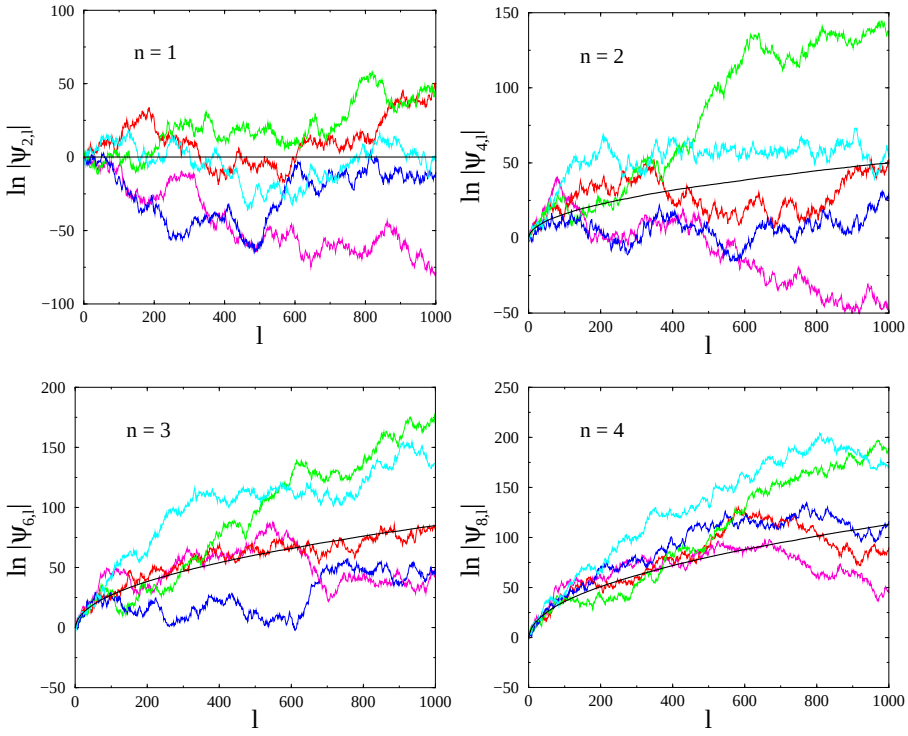

Figure 7. Logarithmic plots of $|\psi_{2n,l}|$ against distance l along each chain, for the special zero-energy eigenstate on the even sublattice of semi-infinite disordered ribbons of width $N = 4$, with a disorder strength $w = 1$. Colors code for five different realizations of disorder. Smooth lines: averages over many samples, growing asymptotically as $A_n\sqrt{l}$ (see (3.24)).

3.2. Zero-energy conductance

In this section we investigate the zero-energy conductance of a disordered zigzag ribbon sample of length L and width N, connected to two leads consisting of semi-infinite clean ribbons of the same width. We shall use the transfer-matrix approach to the electronic conductance [22, 23, 24, 25, 26]. Let us start with a brief reminder of this formalism. The $2N \times 2N$ transfer matrix T_E describing the propagation across *one unit cell* of a clean ribbon at energy E is obtained by recasting the tight-binding

equations (2.2) into the form

$$\psi_{m,l+1} = \sum_{n=1}^{2N} (T_E)_{m,n} \psi_{n,l}. \tag{3.28}$$

Taking for definiteness the example of $N = 2$, we thus obtain

$$T_E = \begin{pmatrix} E^2-1 & -E & 1 & -E \\ E & -1 & 0 & 0 \\ 0 & 0 & -1 & E \\ -E & 1 & -E & E^2-1 \end{pmatrix}. \tag{3.29}$$

Looking for an eigenvalue of T_E of the form $y = \mathrm{e}^{\mathrm{i}q}$, we obtain the dispersion law

$$2(1+\cos q) = \gamma^2 = E^2 \pm E, \tag{3.30}$$

with the notation (2.5). The above expression agrees with (2.7) and (2.8). Right at zero energy, the transfer matrix

$$T_0 = \begin{pmatrix} -1 & 0 & 1 & 0 \\ 0 & -1 & 0 & 0 \\ 0 & 0 & -1 & 0 \\ 0 & 1 & 0 & -1 \end{pmatrix} \tag{3.31}$$

is not diagonalizable. Indeed, its characteristic polynomial reads $(y+1)^4$, whereas the eigenvalue $y = -1$, corresponding to the boundaries of the Brillouin zone ($q = \pm\pi$), has only two independent eigenvectors,

$$V_- = \begin{pmatrix} 1 \\ 0 \\ 0 \\ 0 \end{pmatrix} \quad \text{and} \quad V_+ = \begin{pmatrix} 0 \\ 0 \\ 0 \\ 1 \end{pmatrix}, \tag{3.32}$$

in correspondence with the two zero-energy Bloch states (2.20). The peculiar structure of T_0 is stable by multiplication. The matrix describing the propagation across a clean ribbon of width $N = 2$ and length L at zero energy indeed reads

$$T_0^L = (-1)^L \begin{pmatrix} 1 & 0 & -L & 0 \\ 0 & 1 & 0 & 0 \\ 0 & 0 & 1 & 0 \\ 0 & -L & 0 & 1 \end{pmatrix}. \tag{3.33}$$

The power-law growth of the elements of T_0^L, is due to the feature that T_0 is not diagonalizable. It is also closely related to the power-law growth of generic zero-energy eigenstates on clean ribbons, investigated in Section 2.2.

Now, let $\mathcal{T}$ be the $2N \times 2N$ transfer matrix describing the propagation across the disordered sample of length L at zero energy. The structure of the tight-binding equations (3.4) and (3.5) implies that the non-zero elements of $\mathcal{T}$ are $\mathcal{T}_{2k,2l}$ for $k \geq l$ and $\mathcal{T}_{2k+1,2l+1}$ for $k \leq l$. For $N = 2$, we thus obtain

$$\mathcal{T} = \begin{pmatrix} \mathcal{T}_{1,1} & 0 & \mathcal{T}_{1,3} & 0 \\ 0 & \mathcal{T}_{2,2} & 0 & 0 \\ 0 & 0 & \mathcal{T}_{3,3} & 0 \\ 0 & \mathcal{T}_{4,2} & 0 & \mathcal{T}_{4,4} \end{pmatrix}. \tag{3.34}$$

The transfer matrix $\mathcal{T}$ reduces to T_0^L in the absence of disorder. The non-zero elements of both matrices are at the same positions, irrespective of the disorder realization.

According to the transfer-matrix approach [22, 23, 24, 25, 26], the dimensionless conductance g_N of the sample (in units of e^2/h and per spin degree of freedom) reads

$$g_N = \sum_{a=1}^{N} \frac{1}{1+x_a}, \tag{3.35}$$

where the subscript N denotes the number of channels (i.e., half the size of the transfer matrix), while the number $a = 1, \ldots, N$ labels the channels, and the x_a are the eigenvalues of the matrix§

$$\mathcal{X} = \frac{1}{4}\left(\mathcal{M}^\dagger\mathcal{M} + (\mathcal{M}^\dagger\mathcal{M})^{-1} - 2\,\mathcal{I}\right), \tag{3.36}$$

where the matrix

$$\mathcal{M} = \mathcal{R}^{-1}\mathcal{T}\mathcal{R} \tag{3.37}$$

is obtained by rotating the transfer matrix $\mathcal{T}$ of the sample to a basis where the transfer matrix T_0 of the leads is diagonal. In other words, the columns of $\mathcal{R}$ are right eigenvectors of T_0.

In the present situation, we are therefore facing an obstacle, as the transfer matrix T_0 is not diagonalizable. This peculiarity is related to the fact that there are only two Bloch states (2.20) at zero energy. A natural way of regularizing the problem consists in considering a small non-zero energy E. The eigenvalues y_a of T_0 can then be derived from the power-law dispersion (2.16) of the central bands, i.e., $Q^{2N} = E^2$. We have therefore

$$y_a = \mathrm{e}^{\mathrm{i}q_a} = -\mathrm{e}^{\mathrm{i}Q_a} \approx -(1 + \mathrm{i}Q_a), \tag{3.38}$$

with

$$Q_a = Q_0\,\zeta^a \quad (a = 1, \ldots, 2N), \tag{3.39}$$

where the momentum scale Q_0 is given by

$$Q_0 = |E|^{1/N}, \tag{3.40}$$

while the complex number

$$\zeta = \mathrm{e}^{\mathrm{i}\pi/N} \tag{3.41}$$

is the first $2N$th root of unity.

The momentum scale Q_0 provides a cutoff length below which zero-energy properties are approximately valid. A finite ribbon of length L can indeed be expected to exhibit zero-energy features for $Q_0 L \ll 1$, and to be effectively far from zero energy in the opposite regime ($Q_0 L \gg 1$).

In order to proceed, it is advantageous to change basis according to the following formulas.

- For $N = 2K$ even, we set

$$\begin{aligned}
&\mathcal{R}_{a,2k+1} = (-1)^k r_{a,4k+1} = \omega_0^{2k}\zeta^{2ka},\\
&\mathcal{R}_{a,2k+2} = (-1)^{k+1} r_{a,4k+3} = \omega_0^{2k+1}\zeta^{(2k+1)a},\\
&\mathcal{R}_{a,2\hat{k}} = \eta(-1)^{k+1} r_{a,4K-4k+2} = \omega_0^{2k-1}\zeta^{(2\hat{k}-1)a},\\
&\mathcal{R}_{a,2\hat{k}+1} = \eta(-1)^{k+1} r_{a,4K-4k} = \omega_0^{2k}\zeta^{2\hat{k}a},
\end{aligned} \tag{3.42}$$

§ $\mathcal{I}$ denotes the $2N \times 2N$ unit matrix.

- For $N = 2K + 1$ odd, we set

$$\begin{aligned}
\mathcal{R}_{a,2k+1} &= (-1)^k r_{a,4k+1} = \omega_0^{2k}\zeta^{2ka},\\
\mathcal{R}_{a,2k+2} &= (-1)^{k+1} r_{a,4k+3} = \omega_0^{2k+1}\zeta^{(2k+1)a},\\
\mathcal{R}_{a,2\hat{k}+1} &= \mathrm{i}\eta(-1)^k r_{a,4K-4k+4} = \omega_0^{2k-1}\zeta^{2\hat{k}a},\\
\mathcal{R}_{a,2\hat{k}+2} &= \mathrm{i}\eta(-1)^{k+1} r_{a,4K-4k+2} = \omega_0^{2k}\zeta^{(2\hat{k}+1)a},
\end{aligned} \tag{3.43}$$

  with the notations $\hat{k} = K + k$, $\eta = \mathrm{sign}(E)$, $\omega_0 = \mathrm{i}Q_0$, and where $r_{a,m}$ denotes the components of the right eigenvector associated with the eigenvalue y_a in the original basis, where sites are labelled $m = 1, \ldots, 2N$.

The above change of basis makes the eigenvectors look much simpler. The matrix $\mathcal{R}$ thus defined indeed factorizes as $\mathcal{R} = \mathcal{Q}\mathcal{F}$, up to inessential phase conventions that we shall not mention explicitly, where

$$\mathcal{Q} = \mathrm{diag}(1, Q_0, \ldots, Q_0^{N-1}, 1, Q_0, \ldots, Q_0^{N-1}), \tag{3.44}$$

while $\mathcal{F}$ is the matrix of the finite Fourier transform, with elements

$$\mathcal{F}_{a,b} = \frac{\zeta^{ab}}{\sqrt{2N}} \quad (a, b = 1, \ldots, 2N). \tag{3.45}$$

We have $\mathcal{F}^\dagger\mathcal{F} = \mathcal{I}$. So, in the $E \to 0$ limit, the matrix

$$\mathcal{M} = \mathcal{R}^{-1}\mathcal{T}\mathcal{R} = \mathcal{F}^\dagger\mathcal{Q}^{-1}\mathcal{T}\mathcal{Q}\mathcal{F} \tag{3.46}$$

is unitarily equivalent to the matrix

$$\lim_{Q_0\to 0} \mathcal{Q}^{-1}\mathcal{T}\mathcal{Q} = \mathrm{diag}(\mathcal{T}_{1,1} \ldots \mathcal{T}_{2N,2N}). \tag{3.47}$$

Therefore, in the $E \to 0$ limit, the eigenvalues of $\mathcal{M}$ coincide with the diagonal elements $\mathcal{T}_{m,m}$. The eigenvalues of $\mathcal{M}^\dagger\mathcal{M}$ then read $|\mathcal{T}_{m,m}|^2$. The first correction to the limit (3.47) is proportional to the momentum scale Q_0 (see (3.40)).

The zero-energy conductance of a disordered ribbon is therefore entirely dictated by the diagonal elements $\mathcal{T}_{m,m}$ of the sample transfer matrix $\mathcal{T}$. The latter matrix elements can be extracted from the recursion relations (3.4), (3.5). Using the notation (3.14), we get

$$\begin{aligned}
|\mathcal{T}_{4k+1,4k+1}| &= \frac{u_{2k+1,0}}{u_{2k+1,L}}\, \mathrm{e}^{-X_{2k+1,L}},\\
|\mathcal{T}_{4k+2,4k+2}| &= \mathrm{e}^{X_{2k+1,L}},\\
|\mathcal{T}_{4k+3,4k+3}| &= \mathrm{e}^{-X_{2k+2,L}},\\
|\mathcal{T}_{4k+4,4k+4}| &= \frac{u_{2k+2,0}}{u_{2k+2,L}}\, \mathrm{e}^{X_{2k+2,L}}.
\end{aligned} \tag{3.48}$$

In the continuum limit introduced in Section 3.1, the above expressions simplify to

$$|\mathcal{T}_{2n-1,2n-1}| \approx \mathrm{e}^{-X_n(\tau)}, \quad |\mathcal{T}_{2n,2n}| \approx \mathrm{e}^{X_n(\tau)}. \tag{3.49}$$

We recall that the $X_n(\tau)$ are independent Brownian motions such that $\overline{X_n^2(\tau)} = 2\tau$, with $\tau = w^2 L$. Using (3.49), we thus obtain the following universal expression for the dimensionless zero-energy conductance of a long disordered sample of length L:

$$g_N = \sum_{n=1}^{N} \frac{1}{\cosh^2 X_n(\tau)}. \tag{3.50}$$

In the case of a single chain ($N = 1$), the formula

$$g = \frac{1}{\cosh^2 X(\tau)} \tag{3.51}$$

is exact for any finite sample and can be derived by elementary means (see (A.12)).

Our prediction (3.50) can therefore be stated as follows: the zero-energy conductance g_N of a long ribbon is the sum of the conductances of N independent chains. This result seems at first sight hardly compatible with the existence of only two zero-energy Bloch states (2.20) on an infinitely long clean ribbon. The power-law dispersion law (2.16) however shows that all channels are marginally open at zero energy, resolving thus the apparent contradiction.

The distribution of the conductance g_N therefore reads‖

$$f(g_N) = \underbrace{f(g) * \cdots * f(g)}_{N \text{ times}}, \tag{3.52}$$

where stars denote convolution products, while the distribution $f(g)$ of the conductance of a single chain is derived in (A.15). The above result is however not very useful for practical purposes. More explicit predictions can be made for short and long samples.

For a weak enough disorder, such that $w^2 L \ll 1$, the result (3.50) simplifies as

$$g_N \approx N - \sum_{n=1}^{N} X_n^2(\tau). \tag{3.53}$$

The distribution of the conductance is therefore peaked around the maximal ballistic value ($g_N = N$), as should be:

$$f(g_N) \approx \frac{(N - g_N)^{(N-2)/2}\, \mathrm{e}^{-(N-g_N)/(4w^2L)}}{\Gamma(N/2)(4w^2L)^{N/2}}. \tag{3.54}$$

We have in particular

$$\overline{g_N} \approx N(1 - 2w^2 L), \quad \mathrm{var}\,(g_N) \approx 8Nw^4L^2. \tag{3.55}$$

The asymptotic behavior of the conductance in the opposite insulating regime ($w^2 L \gg 1$) can be investigated as follows. Typically, i.e., for most realizations of disorder, the result (3.50) is dominated by the best conducting chain. We thus have

$$g_N \approx 4\, \mathrm{e}^{-2|X_{\min}(\tau)|}, \tag{3.56}$$

where $|X_{\min}(\tau)|$ is the smallest absolute value of the N Brownian motions. The latter quantity reads

$$|X_{\min}(\tau)| = 2w\sqrt{L}\, z_N, \tag{3.57}$$

and so

$$\ln g_N \approx \ln 4 - 4w\sqrt{L}\, z_N, \tag{3.58}$$

where z_N is the smallest of N independent random numbers x_n, drawn from the normalized half-Gaussian law

$$f(x) = \frac{2}{\sqrt{\pi}}\, \mathrm{e}^{-x^2} \quad (x > 0). \tag{3.59}$$

‖ We use the notation $f(g)$ for the distribution (probability density) of g, as a shorthand for $f_g(g)$, whenever there is no ambiguity.

The distribution of z_N can be obtained by means of a standard argument from extreme-value statistics [36]. We have $\mathrm{Prob}\{x_n > x\} = \operatorname{erfc} x$, where

$$\operatorname{erfc} x = \frac{2}{\sqrt{\pi}} \int_x^\infty \mathrm{e}^{-x'^2}\, \mathrm{d}x' \tag{3.60}$$

is the complementary error function, and so $\mathrm{Prob}\{z_N > z\} = (\operatorname{erfc} z)^N$, and

$$f(z_N) = \frac{\mathrm{d}}{\mathrm{d}z_N}(\operatorname{erfc} z_N)^N = \frac{2N}{\sqrt{\pi}}\, \mathrm{e}^{-z_N^2}(\operatorname{erfc} z_N)^{N-1}. \tag{3.61}$$

The scaling behavior of the distribution of $\ln g_N$ for typical long samples is readily obtained by inserting the distribution (3.61) into the formula (3.58):

$$\begin{aligned} f(\ln g_N) \approx{}& \frac{N}{\sqrt{4\pi w^2 L}}\, \exp\left(-\frac{(\ln 4 - \ln g_N)^2}{16 w^2 L}\right) \\ &\times \left(\operatorname{erfc} \frac{\ln 4 - \ln g_N}{4w\sqrt{L}}\right)^{N-1}. \end{aligned} \tag{3.62}$$

We have in particular

$$\overline{\ln g_N} \approx \ln 4 - C_N w\sqrt{L}, \quad \operatorname{var}(\ln g_N) \approx D_N w^2 L, \tag{3.63}$$

with

$$C_N = 4\,\overline{z_N}, \quad D_N = 16\left(\overline{z_N^2} - \overline{z_N}^2\right) \tag{3.64}$$

and

$$\overline{z_N} = \int_0^\infty (\operatorname{erfc} z)^N\, \mathrm{d}z, \quad \overline{z_N^2} = \int_0^\infty 2z(\operatorname{erfc} z)^N\, \mathrm{d}z. \tag{3.65}$$

The latter expressions have been derived from (3.61) by means of integrations by parts.

The formulas (3.62) and (3.63) constitute the main results of this section. It is clear from their derivation that they hold for all values of the disorder strength w. We thus predict that the typical zero-energy conductance g_N of a disordered sample decays as $\exp(-C_N w\sqrt{L})$ (i.e., subexponentially) with its length L. Moreover, the conductance distribution is far from the conventional log-normal form suggested by the one-parameter scaling theory of Anderson localization. Indeed the relative variance of $\ln g_N$ approaches a non-trivial constant:

$$\frac{\operatorname{var}(\ln g_N)}{\left(\overline{\ln g_N}\right)^2} \to K_N = \frac{D_N}{C_N^2}. \tag{3.66}$$

For the first values of N, the moments involved in (3.64) can be worked out explicitly. We thus get

$$C_1 = \frac{4}{\sqrt{\pi}}, \quad D_1 = 8 - \frac{16}{\pi}, \quad K_1 = \frac{\pi}{2} - 1 \tag{3.67}$$

and

$$\begin{aligned} &C_2 = \frac{8 - 4\sqrt{2}}{\sqrt{\pi}}, \quad D_2 = 8 - \frac{16}{\pi}(7 - 4\sqrt{2}), \\ &K_2 = \frac{\pi}{4}(3 + 2\sqrt{2}) - \frac{5}{2} - \sqrt{2}. \end{aligned} \tag{3.68}$$

For wide ribbons ($N \gg 1$), the distribution (3.61) of z_N becomes a narrow exponential:

$$f(z_N) \approx \frac{2N}{\sqrt{\pi}}\, \exp\left(-\frac{2N z_N}{\sqrt{\pi}}\right). \tag{3.69}$$

We thus obtain the following limits as $N \to \infty$:

$$NC_N \to \sqrt{4\pi}, \quad N^2 D_N \to 4\pi, \quad K_N \to 1. \tag{3.70}$$

Figure 8 shows plots of NC_N, $N^2 D_N$ and K_N against the ribbon width N. Horizontal lines show the limits (3.70). Figure 9 shows a plot of $\overline{\ln g_N}$ against $w\sqrt{L}$, for ribbon widths up to $N = 6$. Each data point has been obtained by averaging the conductance g_N, as given by the universal expression (3.50), over 10^7 realizations of disorder. Straight dashed lines show the asymptotic result (3.63). All the curves for $N \geq 3$ present an inflection point.

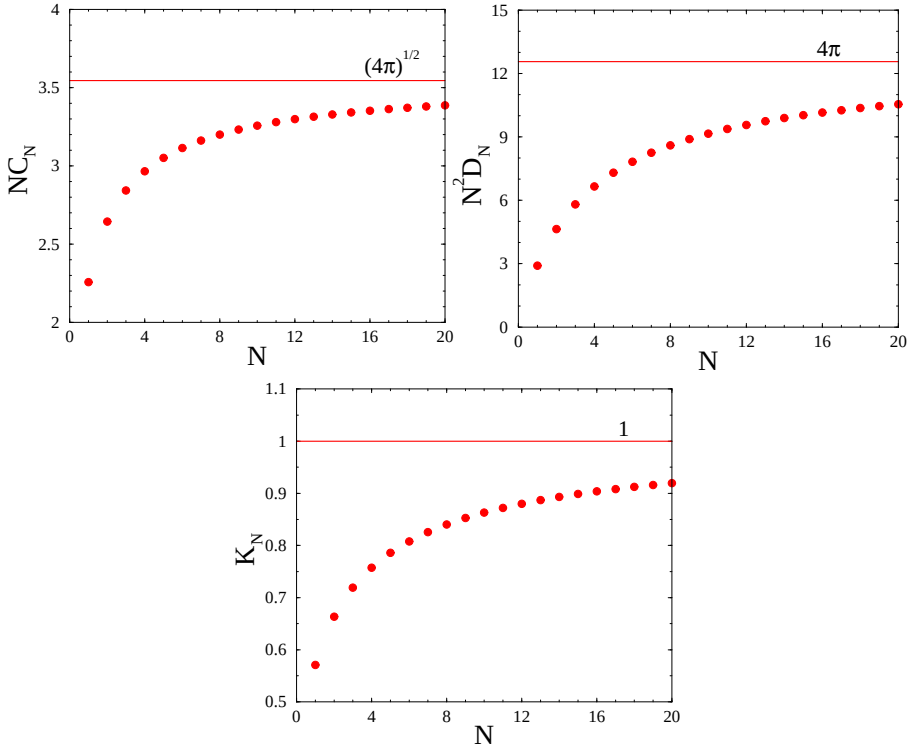

Figure 8. Plots of the constants NC_N, $N^2 D_N$ and K_N against ribbon width N. Horizontal lines: asymptotic limits (3.70).

We close with a few illustrations of the full distribution of the zero-energy conductance g_N, as given by the universal expression (3.50). The forthcoming histograms have been obtained from 10^7 independent realizations of disorder. Figure 10 shows the distribution of g_N for $N = 2$ and $N = 4$ and several values of $\tau = w^2 L$. Near the maximal ballistic conductance ($g_N \to N$), the quadratic approximation (3.53) holds, and so the distribution has the power-law behavior of (3.54), i.e.,

$$f(g_N) \approx \frac{(N - g_N)^{(N-2)/2}}{\Gamma(N/2)(4w^2 L)^{N/2}}. \tag{3.71}$$

This explains why the plotted distributions have finite limiting values for $N = 2$, while they vanish linearly for $N = 4$. The conductance distributions also exhibit internal

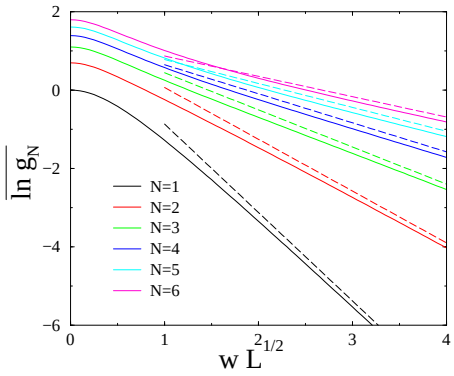

Figure 9. Plot of $\overline{\ln g_N}$ against $w\sqrt{L}$, for ribbon widths $N = 1$ to 6 (bottom to top). Straight dashed lines: exact asymptotic behavior (3.63).

singularities at integer values of the conductance ($g_N = 1, 2, \ldots$), in correspondence with channel thresholds. Figure 11 shows the distribution of $\ln g_N$ for $N = 2$ and $N = 4$ and $w^2L = 100$. The histograms (black curves) consist of a smooth background, which is reproduced to a very high accuracy by our analytical prediction (3.62) (red curves), and of a narrow peak corresponding to $g_N = 1$. The height of this peak exceeds the vertical scale of the plot, while the peaks at higher integer values of g_N are not visible.

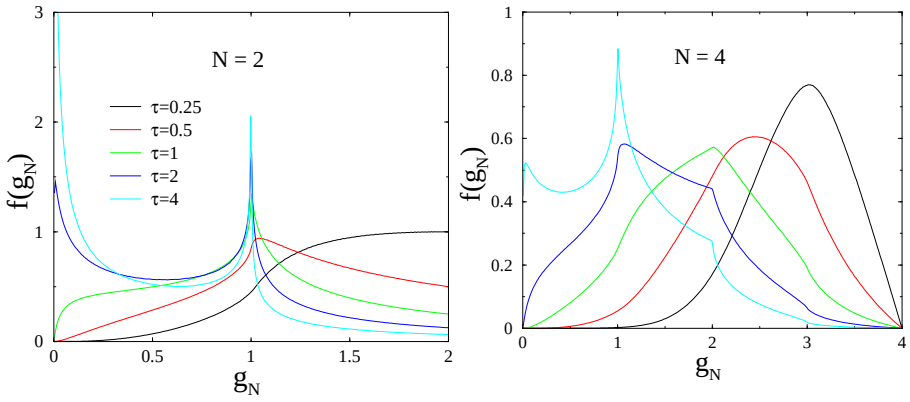

Figure 10. Distribution $f(g_N)$ of the zero-energy conductance for widths $N = 2$ and $N = 4$ and several values of $\tau = w^2L$ (the color code is common to both panels).

4. Discussion

The present paper comes after many earlier works devoted to the electronic properties of zigzag nanoribbons [5, 6, 7, 8, 9, 10, 11, 12, 13, 14, 15, 16, 17, 18, 19, 20]. It is therefore useful to sum up our main findings.

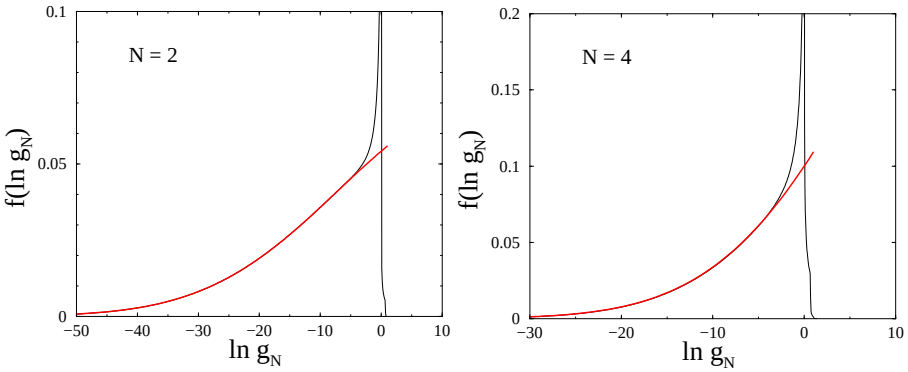

Figure 11. Distribution of $\ln g_N$ for $N = 2$ and $N = 4$ and $w^2 L = 100$. Black curves: histograms. Red curves: analytical prediction (3.62).

As far as clean ribbons are concerned (Section 2), our main point has been to emphasize the role of the unusual power-law dispersion of the central bands. The wings of these bands have been known for long to consist of localized edge states. The associated power-law dispersion (2.16), with its exponent equal to the width N of the ribbon, seems however to have been noticed so far only in [17]. This scaling result has several far reaching consequences. It is in particular responsible for the strong power-law divergence (2.17) of the density of states near zero energy, and for the vanishing of the localization length of the edge states (2.19). Another characteristic property of clean ribbons is the existence of only two zero-energy Bloch states (2.20), irrespective of the ribbon width. A related matter concerns the structure of generic zero-energy eigenstates in a semi-infinite geometry. These eigenstates grow as various powers of the distance to the end of the ribbon (see (2.28)).

For a finite ribbon of length L, these zero-energy features are only valid in a tiny neighborhood of zero energy, defined by the condition $Q_0 L \ll 1$, where the momentum scale reads $Q_0 = |E|^{1/N}$ (see (3.40)). In the situation where the numerical calculations reported in [20] have been performed, i.e., $N = 8$ and $E = 10^{-6}$, we predict a surprisingly sizeable momentum $Q_0 = 0.18$, in spite of the very small nominal value of energy. The system is therefore effectively far from zero energy as soon as its length L exceeds the very modest length of $1/Q_0 \sim 6$ units, shorter than its width. This may explain why the beauties described in the present work were not unveiled by the numerical approach used in [20].

In the presence of hopping (off-diagonal) disorder, which respects the lattice chiral symmetry (Section 3), our leitmotiv is that all zero-energy localization properties are anomalous, for arbitrary values of the disorder strength w. As a matter of fact, all observables which would either grow or decay exponentially in the case of conventional Anderson localization exhibit an anomalous subexponential behavior on disordered zigzag ribbons at zero energy. This holds especially for typical wavefunctions of generic eigenstates in a semi-infinite geometry, which grow exponentially as a function of $w\sqrt{l}$ (see (3.24)), and for the typical conductance of finite disordered samples of length L, which falls off exponentially as a function of $w\sqrt{L}$ (see (3.63)). These exact scaling results involve constants A_n, B_n, C_N and D_N which depend only on the channel number n or on the ribbon width N. We have derived the exact constants C_N and D_N

by means of extreme-value statistics. It would be desirable to find out an analytical way of deriving the asymptotic behavior (3.27) of the constants A_n and B_n.

These findings can be put in perspective with zero-energy properties of disordered strips made of N coupled channels [32, 33, 34, 35]. In the latter case, with off-diagonal disorder, localization properties have been shown to be conventional whenever N is even, and unconventional whenever N is odd, with subexponential scaling properties germane to those we have found on zigzag ribbons. Ribbons and strips could be expected to have some common features. Indeed the situation of a single chain, investigated by elementary means in Appendix A, can be recovered as the particular case $N = 1$ of both ribbons and strips. The plenty of analytical results derived in this paper however testifies that zigzag ribbons lend themselves to many exact calculations, which would just not be possible in other geometries, including strips or armchair ribbons.

Finally, from the viewpoint of the transfer-matrix formalism, disordered zigzag ribbons provide an interesting case study with many unusual features. The transfer matrix T_0, describing electron propagation through one unit cell of a clean ribbon at zero energy, is not diagonalizable. This property originates in the existence of only two zero-energy Bloch states, irrespective of the ribbon width. These features have a remarkable consequence, namely the power-law growth of generic zero-energy eigenstates in a semi-infinite geometry. In the presence of hopping (off-diagonal) disorder, the elements of the matrix products $\mathcal{T}$, describing propagation through whole disordered samples, exhibit an anomalous subexponential growth, related to the similar growth of generic eigenstates and to the subexponential falloff of the conductance. It is worth recalling that, in a situation exhibiting conventional Anderson localization, the matrix product $\mathcal{T}$ would grow as $\exp(\gamma L)$, with $\gamma > 0$ being the largest Lyapunov exponent of the matrix product. In the present case of zigzag ribbons with off-diagonal disorder at zero energy, the subexponential growth of $\mathcal{T}$ implies that γ vanishes. To sum up, we have thus explicitly constructed non-trivial random matrix products such that all Lyapunov exponents vanish identically.

Acknowledgments

It is a pleasure to thank Cristina Bena, Jean-Noël Fuchs and Gilles Montambaux for fruitful discussions. The research of YA is partially supported by grant 400/2012 of the Israeli Science Foundation.

Appendix A. Zero-energy properties of a disordered chain

In this Appendix we study by elementary means various zero-energy properties of a tight-binding chain with off-diagonal disorder [27, 28, 29, 31]. We consider the Hamiltonian

$$\mathcal{H} = \sum_n t_n (a_{n-1}^\dagger a_n + a_n^\dagger a_{n-1}) \tag{A.1}$$

on a disordered segment of length $2L$ embedded in a clean chain, as shown in Figure A1.

We parametrize the hopping amplitudes of the disordered segment as

$$t_{2l-1} = u_l = \exp\bigl(\varepsilon_l^{(u)}\bigr), \quad t_{2l} = v_l = \exp\bigl(\varepsilon_l^{(v)}\bigr), \tag{A.2}$$

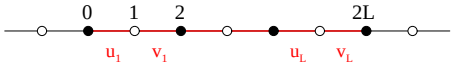

Figure A1. A disordered segment embedded in a clean chain. Black lines: clean bonds with unit hopping amplitudes ($t_n = 1$). Red lines: disordered bonds with random hopping amplitudes ($t_n = u_l$ or v_l).

where the $\varepsilon_l^{(u,v)}$ are again independent random variables, drawn from an unspecified symmetric probability distribution such that $\overline{\varepsilon_l} = 0$ and $\mathrm{var}\,(\varepsilon_l) = w^2$. The disordered sample is connected to two clean semi-infinite leads ($t_n = 1$).

Wavefunction

At zero energy, the amplitudes of the wavefunction at even sites (full symbols) and odd sites (empty symbols) of the disordered sample decouple and obey the recursions

$$\begin{aligned} &u_l\psi_{2l-2} + v_l\psi_{2l} = 0, \\ &v_l\psi_{2l-1} + u_{l+1}\psi_{2l+1} = 0. \end{aligned} \tag{A.3}$$

These amplitudes therefore read [27, 28, 29, 31]

$$\psi_{2l} = (-1)^l \frac{U_l}{V_l}\psi_0, \quad \psi_{2l+1} = (-1)^l \frac{u_1}{u_{l+1}}\frac{V_l}{U_l}\psi_1 \tag{A.4}$$

in terms of the initial values ψ_0 and ψ_1, where we have introduced the products

$$U_l = \prod_{k=1}^{l} u_k, \quad V_l = \prod_{k=1}^{l} v_k. \tag{A.5}$$

Reflection, transmission, and conductance

In order to calculate the reflection and transmission amplitudes r and t of the disordered sample at zero energy, we impose the following wavefunction in the leads

$$\psi_n = \begin{cases} \mathrm{e}^{\mathrm{i}qn} + r\,\mathrm{e}^{-\mathrm{i}qn} & (n \le 0), \\ t\,\mathrm{e}^{\mathrm{i}q(n-2L)} & (n \ge 2L), \end{cases} \tag{A.6}$$

describing the scattering of a particle incoming from the left with momentum q (at zero energy, we have $q = \pi/2$).

First, using the second line of (A.3) for $l = 0$ and $l = L$, we obtain the four boundary amplitudes:

$$\begin{aligned} &\psi_0 = 1 + r, \quad \psi_1 = \frac{\mathrm{i}(1-r)}{u_1}, \\ &\psi_{2L-1} = -\frac{\mathrm{i}t}{v_L}, \quad \psi_{2L} = t. \end{aligned} \tag{A.7}$$

Then, using (A.4), we can express the reflection and transmission amplitudes in terms of the products V_L and U_L:

$$r = \frac{V_L^2 - U_L^2}{V_L^2 + U_L^2}, \quad t = (-1)^L \frac{2V_L U_L}{V_L^2 + U_L^2}. \tag{A.8}$$

These reflection and transmission amplitudes are real. They obey $r^2 + t^2 = 1$, as should be. The reflection amplitude r vanishes if the equality

$$U_L = V_L \tag{A.9}$$

is fulfilled. This is the condition on the disorder realization for the disordered segment of length $2L$ to admit an exact zero-energy eigenstate with either periodic (if L is even) or anti-periodic (if L is odd) boundary conditions. We have then $t = (-1)^L$.

Introducing the quantity

$$X_L = \ln \frac{V_L}{U_L} = \sum_{l=1}^{L} \ln \frac{v_l}{u_l} = \sum_{l=1}^{L} \left(\varepsilon_l^{(v)} - \varepsilon_l^{(u)} \right), \tag{A.10}$$

the expressions (A.8) can be recast as

$$r = \tanh X_L, \quad t = \frac{(-1)^L}{\cosh X_L}. \tag{A.11}$$

The dimensionless conductance of the disordered segment at zero energy is therefore exactly given by

$$g = t^2 = \frac{1}{\cosh^2 X_L}. \tag{A.12}$$

In the regime of long samples ($L \gg 1$), the rightmost side in (A.10) is the sum of $2L$ independent random variables with zero mean and variance w^2. Hence X_L behaves asymptotically as a Gaussian variable with zero mean and variance 2τ, where we have introduced the shorthand

$$\tau = w^2 L. \tag{A.13}$$

The distribution of X_L therefore reads

$$f(X_L) = \frac{\mathrm{e}^{-X_L^2/(4\tau)}}{\sqrt{4\pi\tau}}. \tag{A.14}$$

The distribution of the conductance g of a long disordered segment can be obtained by changing variables from X_L to g in (A.14). We thus obtain the following universal asymptotic result:

$$f(g) = \frac{1}{4g\sqrt{\pi\tau(1-g)}} \exp\left(-\frac{1}{4\tau} \left(\ln \frac{1+\sqrt{1-g}}{\sqrt{g}} \right)^2 \right), \tag{A.15}$$

where the disorder strength only enters through τ.

Transfer-matrix formalism

Our last goal is to check that the result (A.12) is correctly predicted by the transfer-matrix formalism exposed in Section 3.2. In the present case, it is advantageous to define the transfer matrix T_n associated with bond number n at zero energy as follows:

$$\begin{pmatrix} t_{n+1}\psi_{n+1} \\ \psi_n \end{pmatrix} = T_n \begin{pmatrix} t_n\psi_n \\ \psi_{n-1} \end{pmatrix}. \tag{A.16}$$

We have explicitly

$$T_n = \begin{pmatrix} 0 & -t_n \\ 1/t_n & 0 \end{pmatrix}. \tag{A.17}$$

The transfer matrices thus defined have unit determinant, and they are statistically independent from each other. The transfer matrix $\mathcal{T}$ describing the propagation across the whole disordered sample reads

$$\mathcal{T} = T_{2L} \ldots T_1 = (-1)^L \begin{pmatrix} \mathrm{e}^{X_L} & 0 \\ 0 & \mathrm{e}^{-X_L} \end{pmatrix}, \tag{A.18}$$

where X_L has been introduced in (A.10).

The transfer matrix T_0 associated with one bond of the leads and a matrix $\mathcal{R}$ of right eigenvectors of T_0 read

$$T_0 = \begin{pmatrix} 0 & -1 \\ 1 & 0 \end{pmatrix}, \quad \mathcal{R} = \begin{pmatrix} \mathrm{i} & -\mathrm{i} \\ 1 & 1 \end{pmatrix}. \tag{A.19}$$

We have therefore

$$\mathcal{M} = \mathcal{R}^{-1}\mathcal{T}\mathcal{R} = (-1)^L \begin{pmatrix} \cosh X_L & -\sinh X_L \\ -\sinh X_L & \cosh X_L \end{pmatrix}. \tag{A.20}$$

The matrix $\mathcal{M}$ thus obtained is real symmetric. The eigenvalues of $\mathcal{M}^\dagger\mathcal{M}$ are therefore the squares of those of $\mathcal{M}$, i.e., $\mathrm{e}^{\pm 2X_L}$. Finally, (3.35) and (3.36) yield the expected result (A.12).

Appendix B. Statistics of zero-energy eigenstates at chain number $n = 2$

In this Appendix we calculate the amplitudes A_2 and B_2 (see (3.26)) which govern the statistics of zero-energy eigenstates on a disordered ribbon for $n = 2$.

Let us introduce the following linear combinations of $X_1(\tau)$ and $X_2(\tau)$:

$$x(\tau) = X_1(\tau) - X_2(\tau), \quad y(\tau) = X_1(\tau) + X_2(\tau). \tag{B.1}$$

The latter processes are independent Brownian motions, so that $\overline{x^2(\tau)} = \overline{y^2(\tau)} = 4\tau$. Moreover, for $n = 2$, (3.21) and (3.22) read

$$M_2(\tau) = m(\tau) = \max_{0 \le \tau' \le \tau} x(\tau') \tag{B.2}$$

and

$$\ln|\psi_{4,l}| \approx m(\tau) + \frac{1}{2}(y(\tau) - x(\tau)). \tag{B.3}$$

The joint distribution of the final position $x(\tau)$ and of the maximum $m(\tau)$ for a single Brownian motion starting at the origin can be determined by the method of images [36]. For an unrestricted Brownian motion starting at a generic position x_0 at time $t = 0$, the probability density of being at position x at time t is given by the free Green's function

$$G(x, \tau; x_0) = \frac{\mathrm{e}^{-(x-x_0)^2/(8\tau)}}{\sqrt{8\pi\tau}}. \tag{B.4}$$

If the Brownian motion is constrained to obey $x(\tau') < m$ for all times $0 < \tau' < \tau$, the probability density is given by the Dirichlet Green's function

$$G_D(x, \tau; x_0) = G(x, \tau; x_0) - G(x, \tau; 2m - x_0), \tag{B.5}$$

constructed from the free one by subtracting the contribution of an image source located at $2m - x_0$. The joint probability density $f(x, m)$ is obtained as

$$f(x, m) = \frac{\partial}{\partial m} G_D(x, \tau; 0) = \frac{(2m - x)\,\mathrm{e}^{-(2m-x)^2/(8\tau)}}{\sqrt{32\pi\tau^3}}. \tag{B.6}$$

This expression holds in the domain defined by the inequalities $m > 0$ and $x < m$.

By integrating the above result over either variable, we obtain the marginal probability density of the other one, namely

$$f_x(x) = \frac{\mathrm{e}^{-x^2/(8\tau)}}{\sqrt{8\pi\tau}}, \quad f_m(m) = \frac{\mathrm{e}^{-m^2/(8\tau)}}{\sqrt{2\pi\tau}} \quad (m > 0). \tag{B.7}$$

The maximum $m(\tau)$ is therefore distributed according to the same half-Gaussian law as the absolute value $|x(\tau)|$ of the last position. The expression (B.6) also yields the joint moments

$$\overline{m(\tau)} = \sqrt{\frac{8\tau}{\pi}}, \quad \overline{m^2(\tau)} = \overline{x^2(\tau)} = 4\tau, \quad \overline{x(\tau)m(\tau)} = 2\tau. \tag{B.8}$$

Inserting the latter expressions into (B.3), we obtain

$$\overline{\ln|\psi_{4,l}|} \approx \overline{m(\tau)} = \sqrt{\frac{8\tau}{\pi}}, \tag{B.9}$$

$$\overline{(\ln|\psi_{4,l}|)^2} \approx \overline{m^2(\tau)} - \overline{x(\tau)m(\tau)} + \frac{1}{2}\,\overline{x^2(\tau)} = 4\tau. \tag{B.10}$$

These results yield the amplitudes A_2 and B_2 announced in (3.26). The last two terms on the right-hand side of (B.10) cancel each other, so that we have $\overline{(\ln|\psi_{4,l}|)^2} \approx \overline{m^2(\tau)}$. This unexpected identity extends neither to higher moments nor to higher n.

References

[1] A. K. Geim and K. S. Novoselov. The rise of graphene. *Nature Materials*, 6:183, 2007.

[2] A. Cresti, N. Nemec, B. Biel, G. Niebler, F. Triozon, G. Cuniberti, and S. Roche. Charge transport in disordered graphene-based low dimensional materials. *Nano Res.*, 1:361, 2008.

[3] A. H. Castro Neto, F. Guinea, N. M. R. Peres, K. S. Novoselov, and A. K. Geim. The electronic properties of graphene. *Rev. Mod. Phys.*, 81:109, 2009.

[4] S. Das Sarma, S. Adam, E. H. Hwang, and E. Rossi. Electronic transport in two-dimensional graphene. *Rev. Mod. Phys.*, 83:407, 2011.

[5] S. P. Mehandru, A. B. Anderson, and J. C. Angus. Hydrogenation of the (1010) graphite edge: Structural considerations from band calculations. *J. Phys. Chem.*, 96:10978, 1992.

[6] M. Fujita, K. Wakabayashi, K. Nakada, and K. Kusakabe. Peculiar localized state at zigzag graphite edge. *J. Phys. Soc. Jpn*, 65:1920, 1996.

[7] K. Nakada, M. Fujita, G. Dresselhaus, and M. S. Dresselhaus. Edge state in graphene ribbons: Nanometer size effect and edge shape dependence. *Phys. Rev. B*, 54:17954, 1996.

[8] L. Brey and H. A. Fertig. Electronic states of graphene nanoribbons studied with the Dirac equation. *Phys. Rev. B*, 73:235411, 2006.

[9] M. Ezawa. Peculiar width dependence of the electronic properties of carbon nanoribbons. *Phys. Rev. B*, 73:045432, 2006.

[10] V. M. Pereira, F. Guinea, J. M. B. Lopes dos Santos, N. M. R. Peres, and A. H. Castro Neto. Disorder induced localized states in graphene. *Phys. Rev. Lett.*, 96:036801, 2006.

[11] M. Kohmoto and Y. Hasegawa. Zero modes and edge states of the honeycomb lattice. *Phys. Rev. B*, 76:205402, 2007.

[12] A. R. Akhmerov and C. W. J. Beenakker. Boundary conditions for Dirac fermions on a terminated honeycomb lattice. *Phys. Rev. B*, 77:085423, 2008.

[13] K. Esaki, M. Sato, M. Kohmoto, and B. I. Halperin. Zero modes, energy gap, and edge states of anisotropic honeycomb lattice in a magnetic field. *Phys. Rev. B*, 80:125405, 2009.

[14] K. Wakabayashi, Y. Takane, M. Yamamoto, and M. Sigrist. Electronic transport properties of graphene nanoribbons. *New J. Phys.*, 11:095016, 2009.

[15] K. Wakabayashi, K. Sasaki, T. Nakanishi, and T. Enoki. Electronic states of graphene nanoribbons and analytical solutions. *Sci. Technol. Adv. Mater.*, 11:054504, 2010.

[16] P. Delplace, D. Ullmo, and G. Montambaux. Zak phase and the existence of edge states in graphene. *Phys. Rev. B*, 84:195452, 2011.

[17] G. Montambaux. Analytical description of edge states in two-component systems. Unpublished, May 2012.

[18] L. Bilteanu, C. Dutreix, A. Jagannathan, and C. Bena. Interplay between edge states and simple bulk defects in graphene nanoribbons. *Eur. Phys. J. B*, 86:240, 2013.

[19] C. Dutreix, L. Bilteanu, A. Jagannathan, and C. Bena. Friedel oscillations at the Dirac cone merging point in anisotropic graphene and graphenelike materials. *Phys. Rev. B*, 87:245413, 2013.

[20] I. Kleftogiannis, I. Amanatidis, and V. A. Gopar. Conductance through disordered graphene nanoribbons: Standard and anomalous electron localization. *Phys. Rev. B*, 88:205414, 2013.
[21] V. M. Pereira, A. H. Castro Neto, and N. M. R. Peres. Tight-binding approach to uniaxial strain in graphene. *Phys. Rev. B*, 80:045401, 2009.
[22] J. L. Pichard and G. André. Many-channel transmission: Large volume limit of the distribution of localization lengths and one-parameter scaling. *EPL*, 2:477, 1986.
[23] K. A. Muttalib, J. L. Pichard, and A. D. Stone. Random-matrix theory and universal statistics for disordered quantum conductors. *Phys. Rev. Lett.*, 59:2475, 1987.
[24] P. A. Mello and J. L. Pichard. Symmetries and parametrization of the transfer matrix in electronic quantum transport theory. *J. Phys. I (France)*, 1:493, 1988.
[25] P. A. Mello, P. Pereira, and N. Kumar. Macroscopic approach to multichannel disordered conductors. *Ann. Phys.*, 181:290, 1988.
[26] C. W. J. Beenakker. Random-matrix theory of quantum transport. *Rev. Mod. Phys.*, 69:731, 1997.
[27] G. Theodorou and M. H. Cohen. Extended states in a one-dimensional system with off-diagonal disorder. *Phys. Rev. B*, 13:4597, 1976.
[28] L. Fleishman and D. C. Licciardello. Fluctuations and localization in one dimension. *J. Phys. C*, 10:L125, 1977.
[29] A. D. Stone and J. D. Joannopoulos. Probability distribution and new scaling law for the resistance of a one-dimensional Anderson model. *Phys. Rev. B*, 24:3592, 1981.
[30] M. Inui, S. A. Trugman, and E. Abrahams. Unusual properties of midband states in systems with off-diagonal disorder. *Phys. Rev. B*, 49:3190, 1994.
[31] J. A. Vergés. Conductance scaling at the band center of wide wires with pure nondiagonal disorder. *Phys. Rev. B*, 65:054201, 2001.
[32] P. W. Brouwer, C. Mudry, B. D. Simons, and A. Altland. Delocalization in coupled one-dimensional chains. *Phys. Rev. Lett.*, 81:862, 1998.
[33] C. Mudry, P. W. Brouwer, and A. Furusaki. Random magnetic flux problem in a quantum wire. *Phys. Rev. B*, 59:13221, 1999.
[34] C. Mudry, P. W. Brouwer, and A. Furusaki. Crossover from the chiral to the standard universality classes in the conductance of a quantum wire with random hopping only. *Phys. Rev. B*, 59:13221, 1999.
[35] P. W. Brouwer, C. Mudry, and A. Furusaki. Nonuniversality in quantum wires with off-diagonal disorder: a geometric point of view. *Nucl. Phys. B*, 565:653, 2000.
[36] W. Feller. *An Introduction to Probability Theory and its Applications*. Wiley, New York, 1966.